Scientific Research Publishing

Open Journal of Applied Sciences, 2024, 14, 1034-1051
https://www.scirp.org/journal/ojapps
ISSN Online: 2165-3925
ISSN Print: 2165-3917

ZnO Incorporated Acrylamide Grafted Chitosan Based Composite Film for Advanced Wound Healing Applications

Khodeja Afrin[1], Kaniz Fatema[1], Fariha Afrose[1], Md. Abdus Samad Azad[1], Md. Shamim Akter[2], Md. Saiful Alam[1], Papia Haque[2], Yeasmin Akter[1*], Newaz Mohammed Bahadur[1*]

[1]Department of Applied Chemistry and Chemical Engineering, Noakhali Science and Technology University, Noakhali, Bangladesh
[2]Department of Applied Chemistry and Chemical Engineering, University of Dhaka, Dhaka, Bangladesh
Email: *yeasmin.acce@nstu.edu.bd, *nmbahadur@yahoo.com

How to cite this paper: Afrin, K., Fatema, K., Afrose, F., Azad, Md.A.S., Akter, Md.S., Alam, Md.S., Haque, P., Akter, Y. and Bahadur, N.M. (2024) ZnO Incorporated Acrylamide Grafted Chitosan Based Composite Film for Advanced Wound Healing Applications. *Open Journal of Applied Sciences*, **14**, 1034-1051.
https://doi.org/10.4236/ojapps.2024.144069

Received: January 16, 2024
Accepted: April 22, 2024
Published: April 25, 2024

Abstract

This study was carried out to prepare ZnO nanoparticles incorporated acrylamide grafted chitosan composite film for possible biomedical application especially drug loading in wound healing. ZnO nanoparticles were prepared by co-precipitation method from zinc acetate di-hydrate and incorporated in acrylamide grafted chitosan. FT-IR and TGA of the prepared composite film confirmed the successful incorporation of ZnO nanoparticles in the acrylamide-grafted polymer matrix. SEM images showed that the ZnO nanoparticles were homogeneously distributed on the porous matrix of the composite film. Water uptake and buffer uptake analysis revealed that the composite film could hold water and buffer sufficiently, which facilitated the absorption of exudate from the wound site. Amoxicillin was loaded in the prepared composite film and the maximum loading efficiency was found to be 67.33% with drug concentration of 300 ppm. *In vitro* studies showed greater antimicrobial activity of drug-loaded composite film compared to both pure film and standard antibiotic disc. Finally, the *In vivo* mouse model showed maximum healing efficiency compared to conventional gauge bandages because the loading of antibiotic in the film produced a synergistic effect and healing time was reduced.

Keywords

Chitosan, ZnO Nanoparticles, Wound Management, Acrylamide Grafting, Bacterial Resistance, Drug Loading

1. Introduction

Wounds are injuries that damage the skin, either due to external factors like accidents or internal factors like metabolic disorders. They are divided according to how severe they are and how long it takes for them to recover. Chronic wounds, such as skin ulcers, take longer to heal due to imbalances in cell production and degradation, while acute wounds, like knife cuts, heal more quickly and efficiently [1]. To repair injured tissue and replace missing tissue, the healing process involves several overlapping and interdependent steps involving different cellular and matrix components [2] [3]. In biology, wound healing is a subprocess of the more general phenomena of cell proliferation and tissue repair. That is why, regenerating damaged tissue during a wound requires a web of interconnected molecular and biological processes [4].

Currently, polymers are playing an important role in all biomedical applications. There has been increasing interest in the use of natural polymers in the last two decades, especially since many notable advances in technology have followed the exploitation of the properties offered by new polymeric materials like blends and composites. Wound dressings are made using several types of polymers, including synthetic, inert, and bioactive polymers. Not only are bioactive polymers biocompatible and biodegradable, but they also actively aid in the healing process at one or more points in the cycle, making them a popular choice. Many of these substances are either intrinsic to the body's matrix or include physiologically active components that aid in wound healing [5]. Chitosan, as a partially deacetylated derivative of chitin, is a unique compound in the preparation of biomaterials for biomedical applications, mainly due to its abundance, biocompatibility, biodegradability, non-toxicity, and antibacterial properties [6]. It is a polysaccharide that has a linear structure and carries a positive charge which is characterized by a combination of β-(1-4)-linked D-glucosamine (deacetylated unit) and N-acetyl-D-glucosamine (acetylated unit) [7] [8] [9]. Chitosan exhibits a broad variety of properties, including various degrees of deacetylation (ranging from 75% - 95%), viscosities, pKa values, and molecular weights (ranging from 50 - 2000 kDa) [10] [11]. It has -NH_2 and -OH groups that can create hydrogen and covalent bonds which opens up a wide range of possibilities for chitosan chemical derivatization [12] [13]. The -OH groups at the C-6 position of chitosan function as Michael donors in alkaline media [14] [15] [16] [17] thus chitosan can tolerate various functional groups, high conversion rates, and favorable reaction rates [18] which enables chitosan to react with acrylonitrile, hydroxyethyl and hydroxypropyl acrylate (two esters of acrylic acid), and acrylamide (AAm), a wide variety of acryl reagents. Moreover, chitosan is one of the most abundant polysaccharides in nature that could be obtained from the shell of crab, shrimp, insects, algae and bacterial cell walls.

Acrylamide, a vinyl-substituted primary amide ($CONH_2$) precursor to polyacrylamides, has excellent biocompatibility and antibacterial properties. Polymers grafted with acrylamide yield in highly hydrophilic materials and tunable

scaffolds for drug delivery systems due to the presence of pendant amide groups. In other words, acrylamide-based composites make excellent wound dressings due to their ability to retain large volumes of water and water-soluble drugs loaded into their matrix [19].

The major problem of wounds is infections which delay wound healing. Nanomaterials show antibacterial activity against these bacteria causing infection in wounds. Metal oxide nanoparticles with tuned size and structure are potential as antibacterial substances and have been of great interest in various biomedical applications [20]. Zinc Oxide (ZnO), an important metal oxide is non-toxic, has large surface area, thermally stable, capable to kill microbes and compatible with biological system. Therefore, bio-nanocomposites made of ZnO nanoparticles might have excellent potential for various biomedical applications and is promising for wound healing [21]. On top of that, combined effect of antibiotic like amoxicillin with metal oxide nanocomposite to cure wound infections could triggered the susceptible bacteria with exceptional efficacy.

This study focused on synthesis, characterization, and application of novel multifunctional composite, having a specific composition optimized according to the targeted applications. The novelty of this work is using biodegradable polymer chitosan for incorporating ZnO nanoparticles obtained from available renewable resources e.g. prawn shells which was low cost and minimal effect on skin upon changing the dressings. Again, in our research, the Michael reaction between chitosan and AAm was performed using an aqueous alkali-urea solution, as opposed to a traditional acidic solution. This specific solution, originally formulated by Zhang *et al.* which was unique for composite preparation [22] [23]. Our findings demonstrated that chitosan's degradation rate in this alkali-urea solution is significantly slower compared to its degradation in acidic environments. In addition, ZnO nanoparticles, which are a key factor in accelerated wound healing and in cellular recognition and adhesion, were conjugated with the grafted polymer network in order to modulate their interaction with various fluids and contact with cells. The influence of different components on the ability of composite to respond to relevant biological media was also investigated. Moreover, the composite capacity to act as a drug carrier and self-healing performance was evaluated by studying the release profiles of amoxicillin, a penicillin-type antibiotic.

2. Experimental

2.1. Resources

A prawn hatchery located in the Satkhira district of the Khulna division in Bangladesh provided the prawn shells used as ingredients to prepare Chitosan flake. Zinc acetate dihydrate ($Zn(CH_3COO)_2{\cdot}2H_2O$, >98%), Urea ($H_2NCONH_2$), Lithium hydroxide monohydrate ($LiOH{\cdot}H_2O$), Hydrochloric acid (HCl), Acetic acid (CH_3COOH), Acrylamide (C_3H_5NO, >99%), Ammonium Hydroxide (NH_4OH, >98%), Sodium hydroxide (NaOH, >98%), were obtained from pur-

chased from Sigma-Aldrich, Germany. All other chemicals and solvents were of analytical grades and used directly without further purification.

2.2. Methods

2.2.1. Chitosan Extraction and Zinc Oxide Nanoparticles Synthesis

The process of obtaining chitosan from discarded prawn shells was conducted using the methodology followed by Rashid *et al.* [24] with some minor adjustments to the process. The waste prawn shells were rinsed with distilled water under 50˚C - 60˚C temperature for an hour, dried at 100˚C in an oven and crushed in a milling machine. The protein was removed from the crushed prawn shell by treating it with a 4% aqueous NaOH solution at a 1:16 (w/w) ratio under 70˚C for 3 hours. Then after filtration washed the residue with water and dried at 105˚C for 24 hours using a natural convection oven. The dried sample stirred with 1:16 (w/w) 1 N HCl for 3 hours, washed and deacetylated through boiling in the 50% (w/w) NaOH solution at a proportion of 1:20 (wt%), under high temperature conditions (80˚C - 100˚C) for 4 hours. The resultant product, chitosan, was rinsed comprehensively using distilled water till it reached a neutral pH and then dried in an oven. **Figure 1** showed the condition of the different phases of yielding chitosan.

Zinc oxide nanoparticles were synthesized with minor modifications to Chen *et al.*'s direct co-precipitation method [25]. To dissolve zinc acetate dihydrate, 50 ml of a 0.5 M HCl mixture was made, and a dropwise addition of 0.5 M NH_4OH solution was carried out under vigorous agitation and maintained pH of 9. The solution was aged for 5 hours at 85˚C and centrifuged at 5000 rpm for 10 - 15 minutes to isolate the particles. The isolated particles were then repeatedly rinsed with distilled water to eliminate any by-products. Finally, the particles were heated to 100˚C for 5 hours in an oven to dry them.

2.2.2. Chitosan-Acrylamide Michael Reaction

0.5 g of Chitosan was mixed in a water-based mixture having 4.8 wt% LiOH and 8 wt% urea in 50 mL of solvent. The solution was then freeze thawed at −20˚C for 24 hours which gave clear transparent solution [14]. Two equivalent/NH_2 acrylamide was added under continuous stirring and HCl was added to neutralize the mixture. Finally, grafted chitosan was collected by centrifugation and then oven-dried at 40˚C [26]. Grafting percentage was determined using following equation-

$$\text{Grafting}(\%) = \left[\left(W_2 - W_1\right)/W_1\right] \times 100$$

where, W_1 represents the initial mass of dry chitosan and W_2 represents the dry mass of grafted chitosan.

2.2.3. Preparation of Composite Film

A solution of acrylamide grafted chitosan-ZnO nanoparticles composite film was prepared by combining acrylamide grafted chitosan and ZnO nanoparticles in a proportion of 1:0.06 (grafted chitosan to ZnO). The grafted chitosan was first

(a) Waste Prawn Shell (b) Chitin (c) Chitosan

Figure 1. Chitosan yielding phases and their conditions.

dissolved in a solution of 1% acetic acid and ZnO nanoparticles were introduced into the grafted chitosan solution under constant stirring with a magnetic agitator for 20 minutes and poured into a Petri dish. The films produced by simple solvent casting undergo drying at 40˚C.

2.3. Characterization

The size of the crystals of ZnO nanoparticles was determined via a Rigaku Ultima IV X-ray diffractometer, Japan equipped with Cu-Kα radiation, scanning diffraction angles of 2θ and scan rates of 5˚/min within the temperature range of 10˚C to 80˚C. The FT-IR 8400S spectrophotometer from Shimadzu Corporation, Japan, was utilized to measure the Fourier transform infrared (FTIR) spectra (transmission) of the individual and composite film specimens within the 4000 - 400 cm^{-1} range. Appropriate quantities of KBr and powdered samples were mixed by grinding them in an agate mortar pellet. The KBr disc-formatted material spectra were obtained in the same spectral range with a 4 cm^{-1} resolution and 30 scans were performed in total. A thermogravimetric analyzer (TGA-50, Shimadzu, Japan) was utilized to assess the film sample's thermal stabilities. The device, featuring an alumina cell and operating under a nitrogen flow of 50 cm^3/min, was capable of detecting temperatures up to 800˚C, with a heating increment of 10˚C /min. To examine external fractures and obtain a profound intellect of the morphological aspects of the composite film, a JEOL JSM-6490LA scanning electron microscope (SEM) was employed, functioning at a voltage acceleration of 20 kV. Before observing, the film exterior was covered with a delicate layer of platinum to boost image clarity.

The swelling behavior of composite film was observed by dipping it in a phosphate buffer solution (PBS) with a pH of 7.4 and the water. To mimic real-life conditions, a simulating model using a Petri dish with an absorbent foam representing a wound's surface was created. The sponge's uneven surface was similar to that of a wound. A delicate layer of liquid was created on the top exterior of the sponge by soaking it in about 20 ml of PBS and 20 ml of water. Film samples (1 cm × 1 cm) were cut and weighed up (W_0), and then positioned on the top exterior of the model. A constant temperature of 37˚C and time interval was applied [27] [28]. The below equation was used to assess the swelling ratio-

$$\text{Swelling}(\%) = \left[\left(W_t - W_0\right)/W_0\right] \times 100$$

where, W_t represents the weights when swollen and W_0 represents the weights when dry. The swelling ratio was calculated by averaging the results of three separate experiments.

The efficiency of the drug loading process was ascertained by UV-visible spectrophotometry (Shimadzu Corporation's UV-1800, Japan) at a wavenumber of 212 nm, enabling precise quantification of the drug concentration. This efficiency, expressed as a percentage, was computed using the methodology outlined using study of Islam *et al.* [29].

The antibacterial assessment study was carried out by Mueller Hinton Agar diffusion method using *S. typhi* and *E. coli* bacteria as test organisms. Bacterial suspension of in colony forming units (CFU)/mL was evenly spread over the surface of the solid agar plates, followed by placing sterilized disk specimens (6 mm diameter) onto them. The plates were incubated at 37˚C for 24 h and then the diameters of the inhibition zones were measured with transparent ruler. A cytotoxicity assay was performed using both Vero cells and BHK-21 cells to evaluate the effects of a bio-nanocomposite in triplicates.

2.4. *In Vivo* Analysis

An experiment was conducted to evaluate the ability of a prepared bio nanocomposite to heal wounds in male mice weighing 25 - 30 grams. This experiment was conducted in full compliance with the European Community Guidelines for animal experimentation and received approval from the University of Dhaka's Institutional Animal Ethics Committee. The mice were kept in a carefully regulated environment, with access to water and subjected to a 12-hour circadian rhythm while being fed a standard pellet diet. The experimental procedure commenced with the administration of ketaride (10 mg/kg) intraperitoneally, inducing anesthesia in the mice for approximately 15 minutes [30]. By shaving the dorsal fur of mice's interscapular region, a cut measuring 1 mm in depth and 1 cm in diameter was made positioned 5 mm from their ears. By removing the epidermal and dermal layers simultaneously, a full-thickness incision was made with minimum bleeding [31]. Treatments included applying 1.5 cm × 1.5 cm patches of drug-infused bio nanocomposite and a typical gauze strip as a control. The surgical procedure was meticulously replicated thrice for each approach, maintaining consistency in wound size. Wound healing assessment encompassed observing re-epithelialization, wound contraction, and wound morphology through concurrent photography. The reduction in wound size was regularly documented, with photographs taken at various stages. The efficiency of wound healing was calculated using a specific formula [32].

$$\text{Healing efficiency}(\%) = \left[\text{Total healedarea}/\text{Total wound area}\right] \times 100$$

3. Results and Discussion

3.1. XRD Analysis ZnO Nanoparticles

XRD analysis was conducted to evaluate the crystalline structure of the synthe-

sized ZnO nanoparticles. **Figure 2** showed the diffraction patterns of ZnO nanoparticles which exhibit intense diffraction peaks at specific angles, namely: 31.72˚ (100), 34.24˚ (002), 36.21˚ (101), 47.49˚ (102), 56.51˚ (110), 62.76˚ (103), 66.32˚ (200), 67.87˚ (130), 69˚ (201), 72.55˚ (004), and 78˚ (202). The spectrum of the synthesized ZnO nanoparticles closely aligns with JCPDS Card No. 36-1451's bulk ZnO, confirming their sole crystalline nature and wurtzite hexagonal structure [33]. By using the Scherrer approximation from the FWHM of the (101) plane reflection, the crystallite size was determined to be 36 nm. The intense and sharp peaks observed in the XRD pattern indicate excellent crystallinity. Furthermore, the ZnO nanoparticles are phase-pure, as no characteristic XRD peaks other than those of ZnO were detected [34].

3.2. FTIR and TGA Analysis of Composite Film

According to **Figure 3**, the absorption spectrum at 1658.78 cm^{-1} in acrylamide moved to 1643.35 cm^{-1} and spectrum at 1654 cm^{-1} in chitosan moved to 1531 cm^{-1}, correspondingly with a concurrent decrease in peak intensity. While this was happening, the absorption spectrum corresponding to the Oxygen-Hydrogen bond stretching that overlapped the Nitrogen-Hydrogen bond stretching of the main amine moved to a smaller number of 2993 cm^{-1}. This peak also broadened, spanning 2900 to 3600 cm^{-1}. These observations suggested an encouraging boost in bonds of hydrogen among acrylamide's -OH chain and chitosan's $-NH_2$ and -OH chains. The presence of these changes indicated a promising level of interactions between molecules and molecular harmony within chitosan and acrylamide. Additionally, the absorption spectrums at 686 cm^{-1} and 586 cm^{-1}, due to amine class's connection to ZnO nanoparticles and the Zn-O stretching mode, respectively, altered significantly. The Zn-O stretching mode moved from 560 cm^{-1} to 586 cm^{-1} upon integration into chitosan-acrylamide network. Given the negative charge on the surface of Zinc oxide nanoparticles, there was an electrostatic interaction involving both the charged positive polar class NH^{3+} of chitosan and the charged negative zinc oxide nanoparticles.

Thermogravimetric analysis was employed to evaluate the heat resistance of individual and composite film. The TGA thermogram for ZnO nanoparticles, bio nanocomposite film, and Chitosan provided both qualitative and quantitative insights into volatile components shown in **Figure 4**. From 23˚C to 800˚C, ZnO nanoparticles exhibited a minimal weight loss of 1.13%, underscoring their high-temperature stability as they barely degraded at 800˚C. The TGA curve of the ZnO nanoparticles incorporated bio nanocomposite film showed decrease in primary weight under 150˚C, attributed to the expulsion of both chemically and physically absorbed fluid [35]. The film began decomposing at a lower temperature than chitosan due to moisture loss. The main chains of acrylamide grafted chitosan started degrading around 230˚C, with final decomposition occurring near 800˚C. The analysis revealed that the majority of the organic layer of the chitosan film (67.85%) decomposed as CO_2 at elevated temperatures. The resid-

ual mass of the film was 16%, indicative of the presence of an inorganic zinc oxide nanoparticle layer. Pure chitosan decomposed completely by 800˚C, with no further degradation beyond 600˚C. These outcomes demonstrated thermal equilibrium of the bio nanocomposite film, which was enhanced by the incorporation of ZnO, due to the heat-resistant nature of the inorganic ZnO nanoparticles, highlighting the film's potential properties for dressing applications.

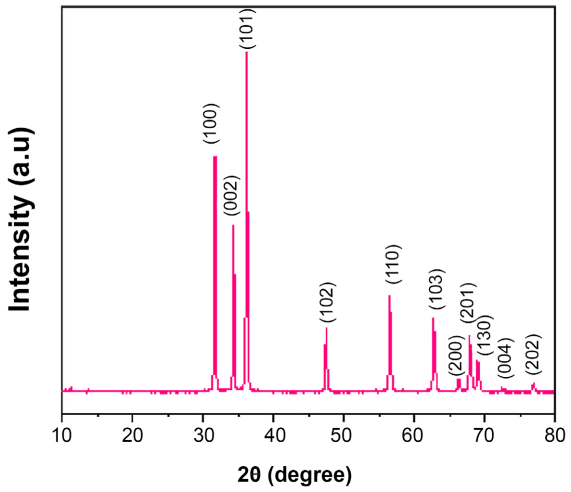

Figure 2. XRD spectra of ZnO nanoparticle.

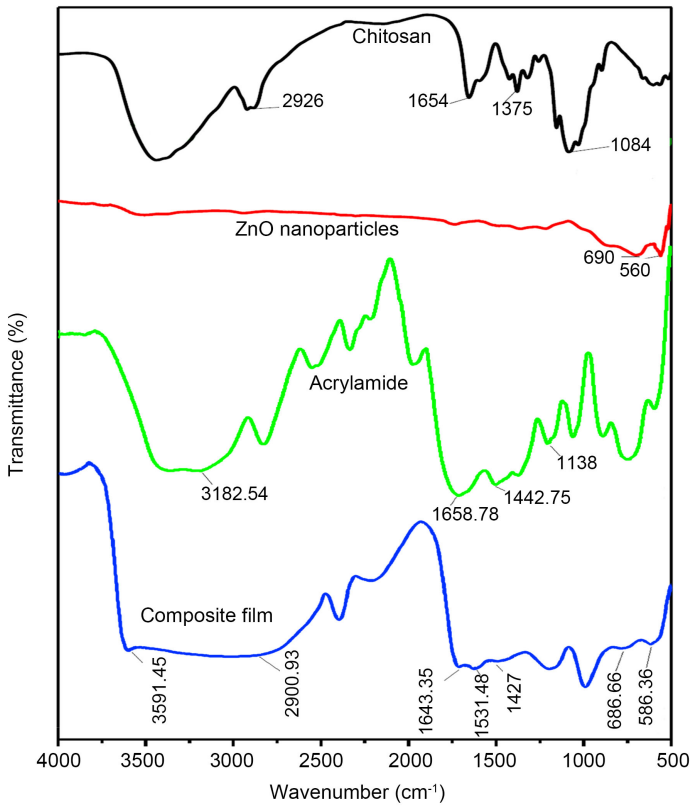

Figure 3. FTIR characterization of composite film, Acrylamide, ZnO nanoparticles, and chitosan.

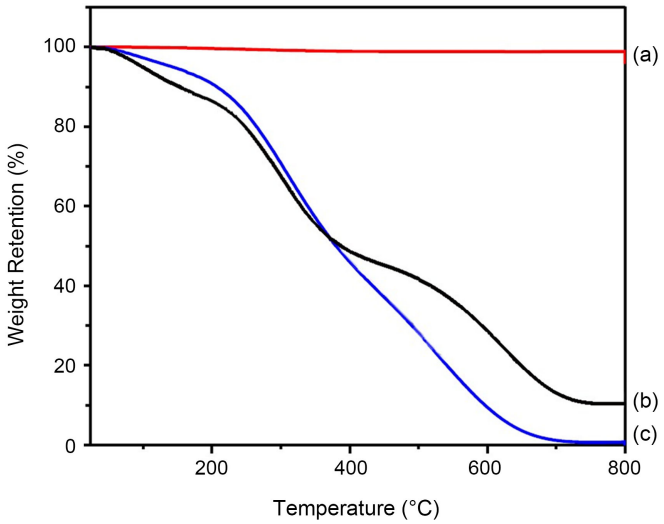

Figure 4. TGA spectra of (a) ZnO nanoparticles, (b) Composite film, (c) Chitosan.

3.3. Morphology and Swelling Behavior

Figure 5 depicted the SEM images of both the bio nanocomposite film and the pure ZnO nanoparticles. SEM image of Zinc oxide nanoparticles (**Figure 5(a)**) showed predominantly monodispersed particles, characterized by spherical shapes. Furthermore, the particle size was discernibly less than 10 μm in comparison to the provided scale. Notably, the ZnO nanoparticles were evenly distributed across the film's surface, exhibiting minimal aggregation (**Figure 5(b)**) and clearly displayed a smooth surface texture, with the ZnO nanoparticles presenting a characteristic spherical-like appearance which confirmed the successful incorporation of ZnO nanoparticles on acryl amide grafted chitosan.

Moreover, bio nanocomposite film demonstrated a marked increase in absorption at 37˚C in both PBS solution with pH 7.4 and distilled water with pH 5.8. In the initial hour, water usage surged, reaching approximately 483% in the buffer solution and about 131% in distilled water shown in **Figure 6(a)**, **Figure 6(b)**. After 10 hours of immersion, both scenarios achieved a state of equilibrium in water capacity. The swelling behavior of a chitosan-based composite film was influenced by factors such as crosslinking, hydrophilicity, and temperature. Particularly at higher pH levels (pH 7.4), the formation of ionic and hydrogen bonds with water molecules played a pivotal role in the film's swelling. These hydrogen bonds contributed to the film's pronounced fluid retention capacity. Notably, the film remained intact, not dissolving. The presence of grafting agents ensured the film maintained its structural integrity post-swelling [36] [37]. Enhanced water uptake in the bio nanocomposite film could be due to the hydronation of NH_2 groupings. Remarkably, the film preserved its form even after 32 hours of immersion in swelling solutions, showing great promise for wound healing applications, particularly in environments mimicking body temperature (37˚C) and blood pH (7.4) [38] [39].

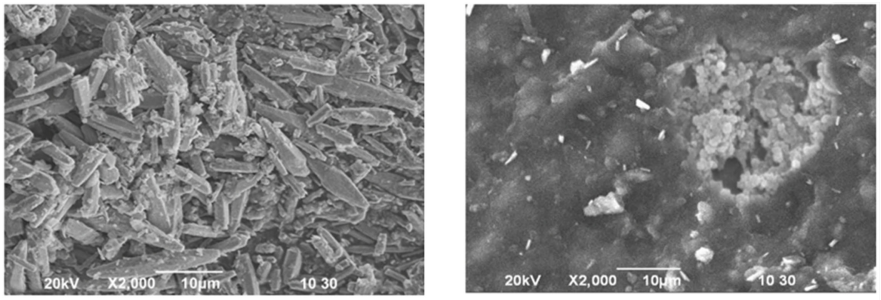

(a) (b)

Figure 5. Scanning Electron Microscope image of (a) ZnO nanoparticles, (b) ZnO incorporated grafted film.

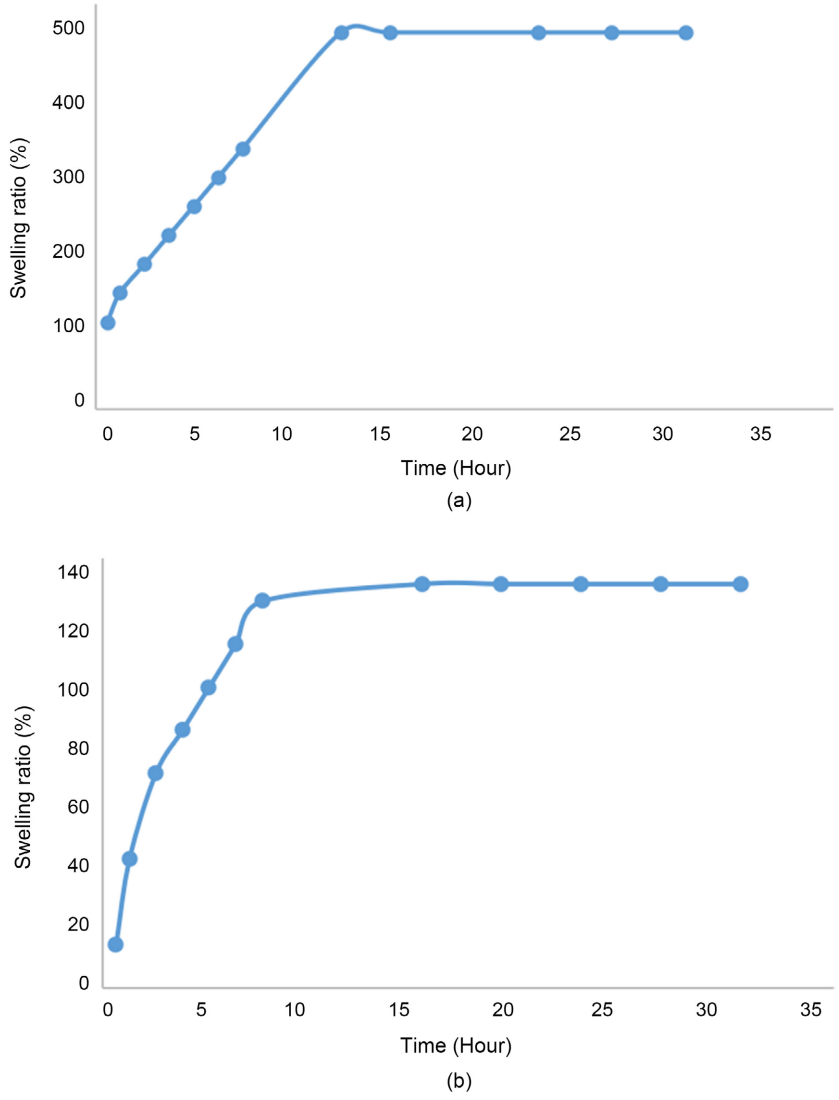

Figure 6. Swelling behavior of bio nanocomposite film in (a) Phosphate buffer and (b) Water.

3.4. Antibacterial Property and Cytotoxicity

The antibacterial efficacy of drug-free and drug-loaded composites were assessed

by calculating their inhibition zones and comparing these findings with a conventional amoxicillin disc. The zones of inhibition measured for the amoxicillin disc, the bio nanocomposite alone, and the amoxicillin-infused bio nanocomposite were 22, 21, and 26 mm against *S. typhi*; and 19, 17, and 23 mm against *E. coli*, respectively (Figure 7). The bio nanocomposite, even without the drug, exhibited antibacterial properties, attributed to the release of ZnO nanoparticles, albeit with a slightly lesser effect compared to the amoxicillin disc. However, the bio nanocomposite loaded with amoxicillin showed the largest inhibition zone in opposition to both types of bacteria which resulted from the combined action of the ZnO nanoparticles and amoxicillin.

On the other hand, cell lines BHK-21 and Vero were used *in vitro* to evaluate the cytotoxicity of bio nanocomposite. Both the control and examined materials did not exhibit any cytotoxicity. The cell lines showed a cell survival rate of above 95% (Table 1). To further evaluate biocompatibility, the samples were cultivated using the Vero cells and BHK-21 fibroblast cell line, with normal culture medium serving as the control. Both cell lines were visible in the optical microscopy pictures (Figure 8) after 48 hours of culture. There was a remarkable improvement as compared to the control in cell viability using the bio nanocomposite, suggesting that it might encourage cell proliferation. Wound repair relies heavily on fibroblasts, and the creation of extracellular matrix proteins which is a valuable step in synchronizing the various stages of wound healing by means of cytokines and growth components [40]. That's why prepared bio nanocomposite showed excellent biocompatibility and exceptional potential for wound dressing film.

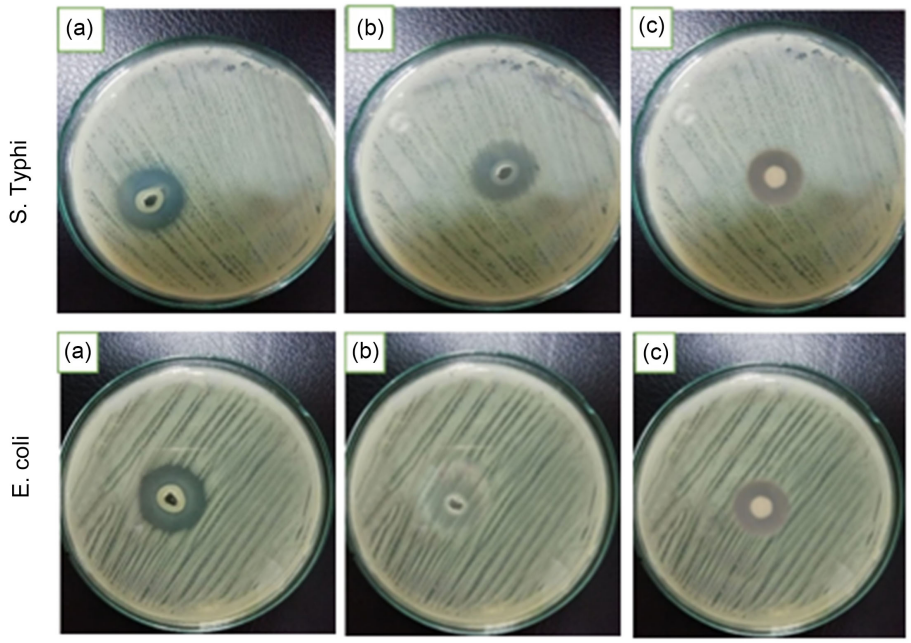

Figure 7. Inhibition zone against *S. typhi* and *E. coli* (a) Drug loaded bio-film, (b) Bio-film (c) Drug.

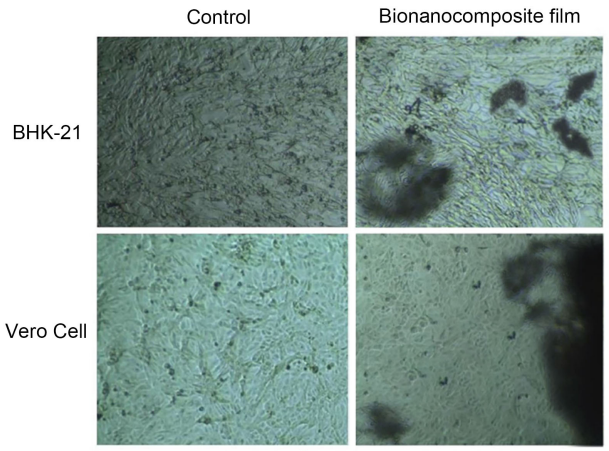

Figure 8. Vero cells and BHK-21 cells under Optical microscope.

Table 1. Cytotoxicity study of prepared bio-nanocomposite.

Trials	Survival percentage	
	Control	Composite film
Vero cells	100%	>95%
BHK-21 cells	100%	>95%
Observations	Cytotoxicity not detected.	Cytotoxicity not detected.

3.5. Drug Loading and Release Efficiency

The focus of this research was to investigate how effective a chitosan/acrylamide bio nanocomposite is at encapsulating amoxicillin. To determine the effectiveness of the loading, the drug-free solution's absorbance levels were monitored at predetermined intervals. Dilution and UV-spectrophotometry were employed to decide the absorbance values at 212 nm of the drug in the solution. Amoxicillin calibration curve at 212 nm was shown in **Figure 9(a)**. A range of amoxicillin concentrations (100 - 1000 ppm) were examined, yielding loading efficiencies of 65%, 63%, 67%, 59%, 46%, and 26%. The highest efficiency, 67%, was observed at an amoxicillin concentration of 300 μg/ml. The grafting process in the bio nanocomposite created cavities that facilitated drug entrapment. At lower drug concentrations, the bio nanocomposite was more effective in trapping molecules, resulting in increased loading efficiency. However, as the concentration of the drug escalated, the entrapment sites reached saturation, leading to a decline in efficiency beyond the 300 μg/ml mark shown in **Figure 9(b)**. The bio nanocomposite's amoxicillin release profile demonstrated that 67% of the medication was discharged after a five-hour duration in PBS at the temperature of 37˚C shown in **Figure 9(c)**. The release mechanisms comprised chitosan chain degradation, acrylamide dissolution, and swelling of the bio nanocomposite. Acrylamide played a key role in hastening the drug's release as it dissolved upon interacting with PBS, thus aiding in the liberation of amoxicillin [14].

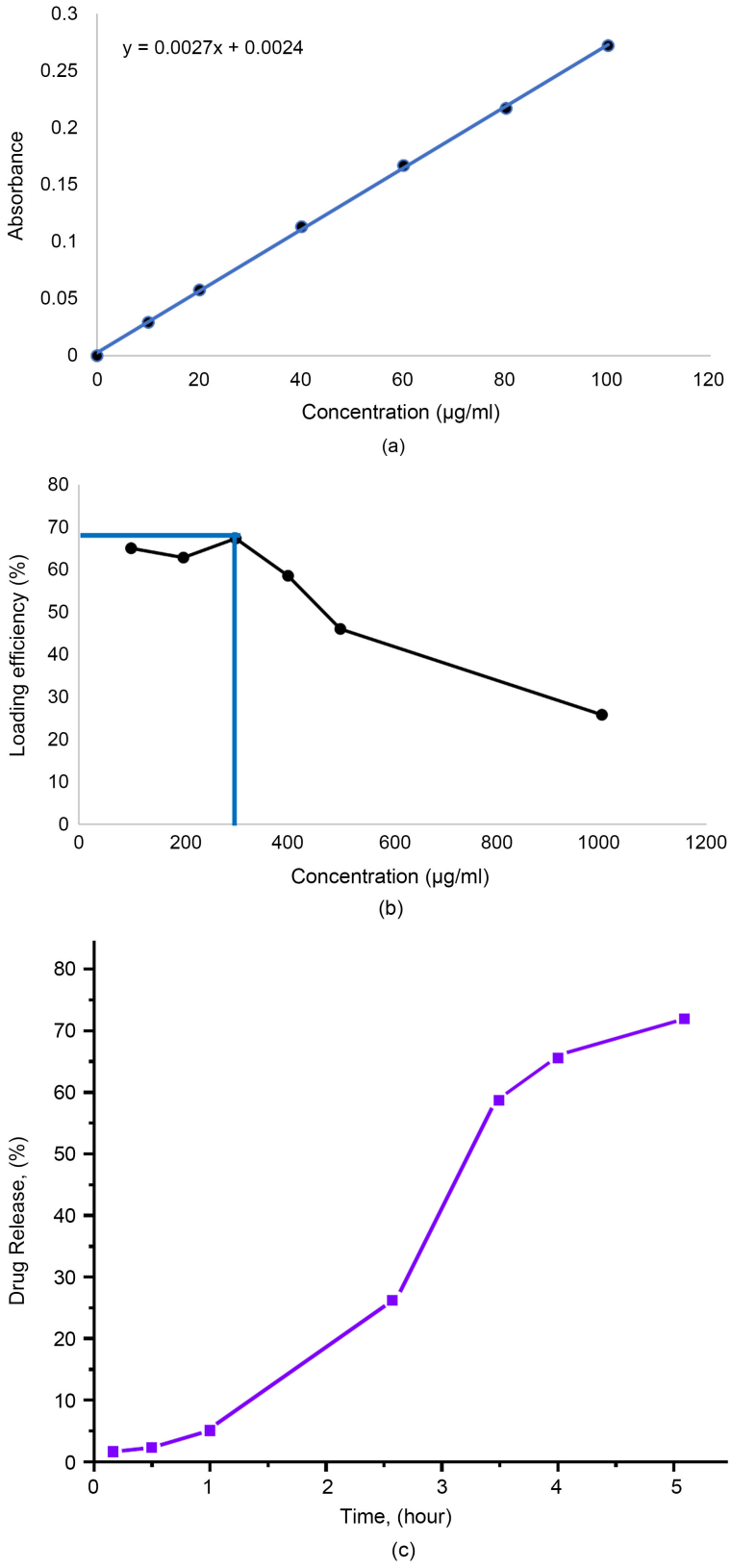

Figure 9. (a) Amoxicillin Calibration Curve at 212 nm via Ultraviolet Spectroscopy, (b) Determining Optimal Loading Efficacy and (c) Amoxicillin Release from Bio-Nanocomposite in pH 7.4 Phosphate Buffer.

Figure 10. Representative images of wounds at various healing times.

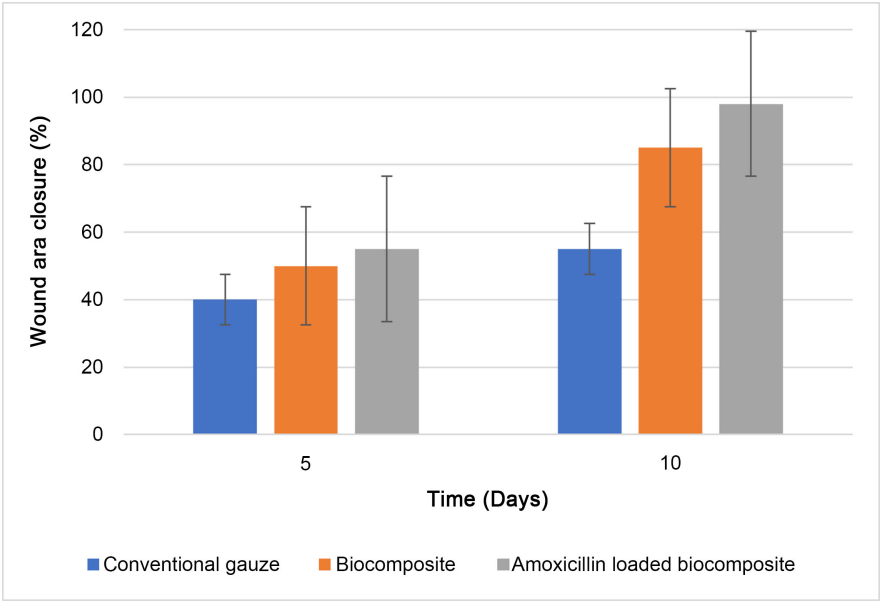

Figure 11. Healing efficiency compared to commercially available gauze bandage per time point per group.

3.6. *In Vivo* Mouse Model

During a 10-day experiment using a mouse model, the wound healing capabilities of a bio nanocomposite film were assessed. The wounds on the mice were treated in groups with drug-infused bio nanocomposite, drug-free bio nanocomposite, and regular gauze for baseline comparison (**Figure 10**). By the fifth

day, the wounds covered with both the drug-loaded and drug-free bio nanocomposites exhibited noticeable wound contraction (50% and 60% respectively) and the formation of granulation tissue. In contrast, wounds treated with regular gauze showed indications of inflammation and minimal tissue formation. After 10 days, wounds cured with the drug-loaded bio nanocomposite achieved complete healing without any scar formation, while those treated with gauze showed clear signs of scarring. The skin treated with the drug-loaded composite appeared smoother, with reduced scabbing, in comparison to both the bio nanocomposite and the control gauze treatments (**Figure 10** and **Figure 11**). The enhanced healing observed with the drug-loaded bio nanocomposite was due to the combined actions of the antibacterial properties of amoxicillin and ZnO nanoparticles, combined with the inherent healing properties of chitosan.

4. Conclusion

In the present study, the composite film prepared by combining ZnO, chitosan, and acrylamide was made using a simple sequential solvent casting approach. Chitosan was extracted from discarded prawn shells, and ZnO nanoparticles were produced by co-precipitation. The FTIR and TGA analyses verified that the ZnO nanoparticles were equally dispersed throughout the material. The bio nanocomposite showed excellent of water and buffer uptake capacity. At a medication concentration of 300 ppm, the film performed an optimum loading efficiency of 67% for amoxicillin. *In vitro* testing revealed that the bio nanocomposite demonstrated superior antibacterial activity compared to both regular amoxicillin and the bio nanocomposite alone when tested against *S. typhi* and *E. coli*. Drug-loaded bio nanocomposite speeded up wound healing *In vivo* more effectively than standard gauze dressing due to the synergistic actions of the medication and ZnO nanoparticles contained within the bio nanocomposite. Overall, prepared occlusive bio nanocomposites film could be a potential wound dressings with excellent biocompatibility and healing capabilities. Hence, this study opens the door for future investigation and identification of the use multifunctional biodegradable polymers in wound dressing films to replace the non-biodegradable commercial gauge bandages to protect the environment from biohazards.

Conflicts of Interest

The authors declare no conflicts of interest regarding the publication of this paper.

References

[1] Anisuzzaman, D., *et al.* (2022) Wound Severity Classification Using Deep Neural Network. arXiv: 2204.07942.

[2] Rothe, M. and Falanga, V. (1989) Growth Factors: Their Biology and Promise in Dermatologic Diseases and Tissue Repair. *Archives of Dermatology*, **125**, 1390-1398. https://doi.org/10.1001/archderm.1989.01670220086015

[3] Shakespeare, P. (2001) Burn Wound Healing and Skin Substitutes. *Burns*, **27**, 517-

522. https://doi.org/10.1016/S0305-4179(01)00017-1

[4] Boateng, J. and Catanzano, O. (2015) Advanced Therapeutic Dressings for Effective Wound Healing—A Review. *Journal of Pharmaceutical Sciences*, **104**, 3653-3680. https://doi.org/10.1002/jps.24610

[5] Karumathil, D.P., Surendran-Nair, M. and Venkitanarayanan, K. (2016) Efficacy of Trans-Cinnamaldehyde and Eugenol in Reducing Acinetobacter Baumannii Adhesion to and Invasion of Human Keratinocytes and Controlling Wound Infection in Vitro. *Phytotherapy Research*, **30**, 2053-2059. https://doi.org/10.1002/ptr.5713

[6] Peppas, N.A. and Buri, P.A. (1985) Surface, Interfacial and Molecular Aspects of Polymer Bioadhesion on Soft Tissues. *Journal of Controlled Release*, **2**, 257-275. https://doi.org/10.1016/0168-3659(85)90050-1

[7] Date, A.A., Hanes, J. and Ensign, L.M. (2016) Nanoparticles for Oral Delivery: Design, Evaluation and State-of-the-Art. *Journal of Controlled Release*, **240**, 504-526. https://doi.org/10.1016/j.jconrel.2016.06.016

[8] Casettari, L., *et al.* (2012) PEGylated Chitosan Derivatives: Synthesis, Characterizations and Pharmaceutical Applications. *Progress in Polymer Science*, **37**, 659-685. https://doi.org/10.1016/j.progpolymsci.2011.10.001

[9] Younes, I. and Rinaudo, M. (2015) Chitin and Chitosan Preparation from Marine Sources. Structure, Properties and Applications. *Marine Drugs*, **13**, 1133-1174. https://doi.org/10.3390/md13031133

[10] Pokhrel, S., Yadav, P.N. and Adhikari, R. (2015) Applications of Chitin and Chitosan in Industry and Medical Science: A Review. *Nepal Journal of Science and Technology*, **16**, 99-104. https://doi.org/10.3126/njst.v16i1.14363

[11] Hao, R., *et al.* (2018) Superior Potassium Storage in Chitin-Derived Natural Nitrogen-Doped Carbon Nanofibers. *Carbon*, **128**, 224-230. https://doi.org/10.1016/j.carbon.2017.11.064

[12] Hamedi, H., Moradi, S., Hudson, S.M. and Tonelli, A.E. (2018) Chitosan Based Hydrogels and Their Applications for Drug Delivery in Wound Dressings: A Review. *Carbohydrate Polymers*, **199**, 445-460. https://doi.org/10.1016/j.carbpol.2018.06.114

[13] Mima, S., Miya, M., Iwamoto, R. and Yoshikawa, S. (1983) Highly Deacetylated Chitosan and Its Properties. *Journal of Applied Polymer Science*, **28**, 1909-1917. https://doi.org/10.1002/app.1983.070280607

[14] Li, C., Han, Q.Y., Guan, Y. and Zhang, Y.J. (2015) Michael Reaction of Chitosan with Acrylamides in an Aqueous Alkali-Urea Solution. *Polymer Bulletin*, **72**, 2075-2087. https://doi.org/10.1007/s00289-015-1390-8

[15] Xie, W., Xu, P. and Liu, Q. (2001) Antioxidant Activity of Water-Soluble Chitosan Derivatives. *Bioorganic & Medicinal Chemistry Letters*, **11**, 1699-1701. https://doi.org/10.1016/S0960-894X(01)00285-2

[16] Xie, W., Xu, P.X., Wang, W. and Liu, Q. (2002) Preparation and Antibacterial Activity of a Water-Soluble Chitosan Derivative. *Carbohydrate Polymers*, **50**, 35-40. https://doi.org/10.1016/S0144-8617(01)00370-8

[17] Alves, N.M. and Mano, J.F. (2008) Chitosan Derivatives Obtained by Chemical Modifications for Biomedical and Environmental Applications. *International Journal of Biological Macromolecules*, **43**, 401-414. https://doi.org/10.1016/j.ijbiomac.2008.09.007

[18] Mather, B.D., Viswanathan, K., Miller, K.M. and Long, T.E. (2006) Michael Addition Reactions in Macromolecular Design for Emerging Technologies. *Progress in Polymer Science*, **31**, 487-531. https://doi.org/10.1016/j.progpolymsci.2006.03.001

[19] Bulut, E. and Turhan, Y. (2021) Synthesis and Characterization of Temperature-Sensitive Microspheres Based on Acrylamide Grafted Hydroxypropyl Cellulose and Chitosan for the Controlled Release of Amoxicillin Trihydrate. *International Journal of Biological Macromolecules*, **191**, 1191-1203. https://doi.org/10.1016/j.ijbiomac.2021.09.193

[20] Salehi, R., *et al.* (2010) Novel Biocompatible Composite (Chitosan-Zinc Oxide Nanoparticle): Preparation, Characterization and Dye Adsorption Properties. *Colloids and Surfaces B*: *Biointerfaces*, **80**, 86-93. https://doi.org/10.1016/j.colsurfb.2010.05.039

[21] Yan, E., *et al.* (2011) Synthesis and Characterization of Fluorescent Chitosan-ZnO Hybrid Nanospheres. *Materials Science and Engineering*: *B*, **176**, 458-461. https://doi.org/10.1016/j.mseb.2011.01.005

[22] Cai, J. and Zhang, L. (2005) Rapid Dissolution of Cellulose in LiOH/Urea and NaOH/Urea Aqueous Solutions. *Macromolecular Bioscience*, **5**, 539-548. https://doi.org/10.1002/mabi.200400222

[23] Cai, J. and Zhang, L. (2006) Unique Gelation Behavior of Cellulose in NaOH/Urea Aqueous Solution. *Biomacromolecules*, **7**, 183-189. https://doi.org/10.1021/bm0505585

[24] Rashid, T.U., *et al.* (2012) A New Approach for The Preparation of Chitosan from γ-Irradiation of Prawn Shell: Effects of Radiation on the Characteristics of Chitosan. *Polymer International*, **61**, 1302-1308. https://doi.org/10.1002/pi.4207

[25] Chen, C., Liu, P. and Lu, C. (2008) Synthesis and Characterization of Nano-Sized ZnO Powders by Direct Precipitation Method. *Chemical Engineering Journal*, **144**, 509-513. https://doi.org/10.1016/j.cej.2008.07.047

[26] Sashiwa, H., *et al.* (2003) Michael Reaction of Chitosan with Various Acryl Reagents in Water. *Biomacromolecules*, **4**, 1250-1254. https://doi.org/10.1021/bm030022o

[27] Dai, M., *et al.* (2009) Chitosan-Alginate Sponge: Preparation and Application in Curcumin Delivery for Dermal Wound Healing in Rat. *BioMed Research International*, **2009**, Article ID: 595126. https://doi.org/10.1155/2009/595126

[28] Vinklárková, L., *et al.* (2017) Film Wound Dressing with Local Anesthetic Based on Insoluble Carboxymethycellulose Matrix. *Journal of Applied Biomedicine*, **15**, 313-320. https://doi.org/10.1016/j.jab.2017.08.002

[29] Islam, M.S., *et al.* (2017) Core-Shell Drug Carrier from Folate Conjugated Chitosan Obtained from Prawn Shell for Targeted Doxorubicin Delivery. *Journal of Materials Science: Materials in Medicine*, **28**, Article No. 55. https://doi.org/10.1007/s10856-017-5859-x

[30] Balakrishnan, B., *et al.* (2005) Evaluation of an *in Situ* Forming Hydrogel Wound Dressing Based on Oxidized Alginate and Gelatin. *Biomaterials*, **26**, 6335-6342. https://doi.org/10.1016/j.biomaterials.2005.04.012

[31] Bhowmik, S., *et al.* (2017) Reinforcement of Gelatin-Based Nanofilled Polymer Biocomposite by Crystalline Cellulose from Cotton for Advanced Wound Dressing Applications. *Polymers*, **9**, Article 222. https://doi.org/10.3390/polym9060222

[32] Parvez, S., *et al.* (2012) Preparation and Characterization of Artificial Skin Using Chitosan and Gelatin Composites for Potential Biomedical Application. *Polymer Bulletin*, **69**, 715-731. https://doi.org/10.1007/s00289-012-0761-7

[33] Patra, P., *et al.* (2014) Ciprofloxacin Conjugated Zinc Oxide Nanoparticle: A Camouflage towards Multidrug Resistant Bacteria. *Bulletin of Materials Science*, **37**, 199-206. https://doi.org/10.1007/s12034-014-0637-6

[34] Sharma, D., *et al.* (2010) Synthesis of ZnO Nanoparticles and Study of Their Antibacterial and Antifungal Properties. *Thin Solid Films*, **519**, 1224-1229. https://doi.org/10.1016/j.tsf.2010.08.073

[35] Mino, G. and Kaizerman, S. (1958) A New Method for the Preparation of Graft Copolymers. Polymerization Initiated by Ceric Ion Redox Systems. *Journal of Polymer Science*, **31**, 242-243. https://doi.org/10.1002/pol.1958.1203112248

[36] Singh, D.K. and Ray, A.R. (1998) Characterization of Grafted Chitosan Films. *Carbohydrate Polymers*, **36**, 251-255. https://doi.org/10.1016/S0144-8617(97)00260-9

[37] Rahman, P.M., Abdul Mujeeb, V.M., Muraleedharan, K. and Thomas, S.K. (2018) Chitosan/Nano ZnO Composite Films: Enhanced Mechanical, Antimicrobial and Dielectric Properties. *Arabian Journal of Chemistry*, **11**, 120-127. https://doi.org/10.1016/j.arabjc.2016.09.008

[38] Mahmud, M., Daik, R. and Adam, Z. (2018) Influence of Poly (Ethylene Glycol) on the Characteristics of γ Radiation-Crosslinked Poly (Vinyl Pyrrolidone)-Low Molecular Weight Chitosan Network Hydrogels. *Sains Malaysiana*, **47**, 1189-1197. https://doi.org/10.17576/jsm-2018-4706-14

[39] Felinto, M.C., *et al.* (2007) The Swelling Behavior of Chitosan Hydrogels Membranes Obtained by UV-and γ-Radiation. *Nuclear Instruments and Methods in Physics Research Section B: Beam Interactions with Materials and Atoms*, **265**, 418-424. https://doi.org/10.1016/j.nimb.2007.09.025

[40] Johnson, Z.I., *et al.* (2019) The Role of Chemokines in Fibrotic Dermal Remodeling and Wound Healing. In: Willis, M.S., Yates, C.C. and Schisler, J.C., Eds., *Fibrosis in Disease*, Humana, Cham, 3-24. https://doi.org/10.1007/978-3-319-98143-7_1